IEEJ Journal of Industry Applications
Vol.6 No.3 pp.205–212 DOI: 10.1541/ieejjia.6.205

Paper

Insulated Signal Transmission System with Near-field Resonant Coupler to Drive High-voltage Power Devices

Hiroshi Shinoda[*a)] Non-member, Takahide Terada[*] Non-member

(Manuscript received May 16, 2016, revised Jan. 6, 2017)

An insulated signal transmission system using a near-field resonant coupler was developed for providing driving signal transmission to control power switching devices. The resonant coupling in the near-field can reduce the unwanted leakage that prevents conventional wireless systems from being deployed inside the metal housing of the switching devices. The focus was on the parasitic capacitance of the resonant coupler because the capacitance needs to be reduced for suppression of the noise current caused by the switching devices. An equivalent circuit model of the resonant coupler was introduced to simulate the capacitance, and validated by showing agreement between the calculated value of 0.76 pF and the measured value of 0.80 pF. An insulated communication module configured with the resonant couplers and two transceivers on the PCB was fabricated. The module demonstrated the switching operation of 3.3 kV–1200 A insulated-gate bipolar transistors (IGBTs) without disturbances between the high-power switching IGBTs and RF transceivers.

Keywords: resonant coupling, near-field, parasitic capacitance, gate driver, PCB, IGBT

1. Introduction

The amount of electrical equipment connected to networks in fields ranging from consumer electronics to social infrastructure has been increasing, and this has caused a significant increase in the number of cables used between the pieces of equipment or between the devices used within them. In particular, the explosive growth in the number of inside cables has interfered with the efforts to downsize equipment, reduce costs, and improve the overall reliability. Moreover, the detachable connectors generally used for cable connections have reliability and cost problems. Therefore, there has been an increasing demand for a new connecting method that enables for connections to be made without exposing the electrode and without needing to have a physical attachment-detachment mechanism. The means for eliminating cables could be considered, such as by using general-purpose wireless communication systems, e.g., wireless LANs. However, these systems suffer from degraded communication quality owing to the diffused reflection of electromagnetic waves on the metallic walls of the equipment.

In providing driving signal transmission to control power electronic equipment such as high voltage inverters [(1)(2)], a high degree of insulation is particularly important in addition to eliminating the cables and connectors as mentioned above. The traditional way of easily obtaining a high insulation for insulated signal transmission is to use signal isolation elements like as optical fibers. However, these fibers are very sensitive to temperature and vibration, which is especially problematic in outdoor applications. Moreover, it is essential to avoid using as many electrical contacts as possible under unfavorable conditions, e.g., the presence of dust or water [(3)(4)]. It is also required to reduce a parasitic capacitance of the signal isolation element for suppression of an electromagnetic interference (EMI) noise caused by power switching devices. When the switching devices such as insulated-gate bipolar transistors (IGBTs) are operated in a power inverter, their high dV/dt rate in the rise time and the fall time causes a noise current in a signal line through the signal isolation element due to its parasitic capacitance between the primary and the secondary.

To address these issues, Nagai et al. introduced a Drive-by- Microwave gate driver which consists of 2.4 GHz GaN/Si transmitter and receiver chips and the butterfly isolation coupler [(5)]. This gate driver can reduce its cost and its size by integrating its components in a printed circuit board based package. They approximately estimated the parasitic capacitance of the butterfly isolation coupler using a theoretical formula of a parallel plate capacitor. For higher-voltage application, however, it is required to analyze the parasitic capacitance more accurately.

The authors previously proposed an insulated signal transmission system using near-field resonant coupling technology [(6)]. The driving signal is transmitted owing to the resonant coupling of two separated planar elements arranged on a multilayer printed circuit board (PCB) with a gate driver circuit. The resonant coupling makes the proposed system better capable of reducing the unwanted leakage to the outside of the board than general wireless communication systems using electromagnetic waves. This makes the system suitable for introduction into power electronic equipment.

Our primary focus for this paper is the design detail of the near-field resonant coupler, including the parasitic capacitance simulation using the equivalent circuit model, which

a) Correspondence to: Hiroshi Shinoda. E-mail: hiroshi.shinoda.xb@hitachi.com
* Research & Development Group, Hitachi, Ltd.
1-280, Higashi-koigakubo, Kokubunji, Tokyo 185-8601, Japan

is different from [5]. In the following sections, we present an insulated signal transmission system using the resonant coupling technology, describe the design of the developed coupler, and discuss the results of our experiments to determine the effectiveness and impact of the coupler.

2. Insulated Signal Transmission System Based on Near-field Resonant Coupling Technology

Figure 1 is a block diagram of an inverter system based on the insulated signal transmission using near-field resonant coupling technology. The IGBT gate drivers convert the driving signals from a logical controller to voltage signals of less than 20 V. These signals are input to an IGBT gate electrode and drive six IGBTs that operate a three-phase motor. In addition, the gate drivers transmit status signals that forward the IGBT on/off status to the logical controller for error detection. While the IGBTs are operating, the collector-to-emitter voltage of the IGBTs and the ground voltage of the gate driver together reach several kilovolts. Therefore, the system requires an insulated signal transmission between the logical controller and the IGBT gate drivers. As the design target, we set an insulated communication module for the insulated signal transmission.

Near-field resonant couplers and RF transceivers are used for the insulated communication module, as shown in Fig. 2. One of the two pairs of couplers is used for the driving signals and the other for the status signals. The pairs are separately arranged on a multilayer PCB. A dielectric layer interposed between the couplers allows the system to maintain a suitable insulation characteristic. The RF transceivers are configured with a transmitting (Tx) circuit and a receiving (Rx) circuit for the microwave band. An amplitude modulation scheme with a low latency characteristic is applied to reduce the propagation delay to less than one hundred nanoseconds for real-time control. The operation frequency of the RF transceivers is set to 2.45 GHz, which is immune from IGBT disturbances because the radiated EMI due to high voltage IGBT switching is generally lower than 0.5 GHz [3]. When a Tx signal has a high signal level, the output from a voltage controlled oscillator (VCO) is transmitted to the coupler because the RF switch is ON. On the other hand, when the Tx signal has a low signal level, the RF switch is turned OFF and the output is cut off. This enables the high/low level signals to be modulated. A detector detects the signals from the couplers and converts them into the voltage that is binarized by a comparator. This enables the high/low level signals to be demodulated. In addition, surge noise filters are supplementarily used to reduce the dV/dt noise currents in the signal line at a connection point between the Tx or Rx circuit and the resonant couplers. The noise current due to the parasitic capacitance of the resonant coupler, can be reduced by a filter comprised of inexpensive chip capacitors and inductors, since the 2.45-GHz signal frequency is considerably higher than the noise current frequency, which is a maximum of 0.1 GHz.

We focused on the insulated communication module and designed the signal level and the propagation delay of it, as shown in Table 1. The values were extracted from data sheet of each component selected from commercially available discrete ICs. Considering the input signal level allowable by each circuit component, the signal level that can be

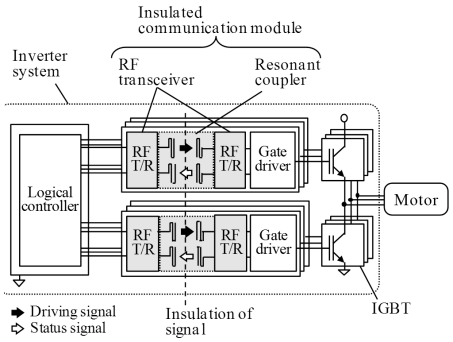

Fig. 1. Block diagram of inverter system based on insulated signal transmission

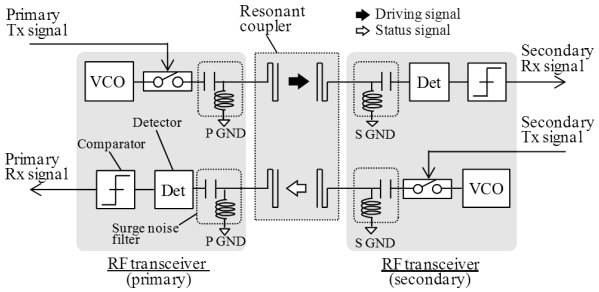

Fig. 2. Block diagram of insulated communication module

Table 1. Estimated signal level and propagation delay of insulated communication module

Component	VCO	RF switch	Surge noise filter	Resonant coupler	Surge noise filter	Detector	Comparator
Each gain	-	> -0.6 dB (ON) < -22 dB (OFF)	-1.0 dB	-0.9 dB	-1.0 dB	-44 mV/dB	-
High signal	-3 dBm	> -3.6 dBm	> -4.6 dBm	> -5.5 dBm	> -6.5 dBm	< 0.3 V	~ 5 V
Low signal	-3 dBm	< -25 dBm	< -26 dBm	< -26.9 dBm	< -27.9 dBm	> 1.2 V	~ 0 V
Each delay	-	10 ns	-	0.3 ns	-	10 ns	30 ns
Total delay	-	10 ns	10 ns	10.3 ns	10.3 ns	20.3 ns	50.3 ns

outputted, and the signal gain in each component, we selected the components so that the signal levels of all the components were within the range where normal operation was possible. The RF switch was selected to satisfy the target specification of 20 dB for the communication signal ratio of high to low. The propagation delay of the resonant coupler was calculated by a high frequency structural simulator (HFSS) which is a commercial finite element method solver for electromagnetic structures in the next section. As a result, we obtained the propagation delay of 50.3 ns which satisfied the target which was set to less than 100 ns.

3. Near-field Resonant Coupler

3.1 Structure and Operation Principles Figure 3 is a schematic of the essential structure of the near-field resonant coupler we proposed. A resonant coupling element configured with a meander pattern and a ground pattern is arranged on both the front and back side of the PCB. The resonant coupling of the two separated elements allows for the signal transmission while maintaining a suitable insulation characteristic. Applying the meander pattern to one portion of the resonator can cancel the radiation component from the pattern since each current flows in the reverse direction at an adjacent conductor of the pattern. The ground pattern

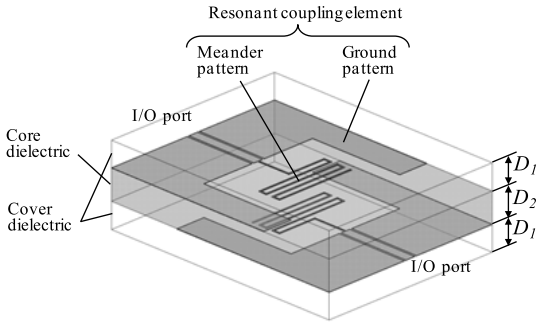

(a) Oblique view of resonant coupler

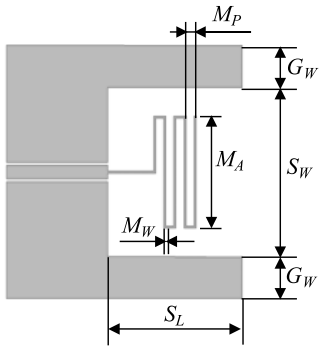

(b) Front view of resonant coupling element

Fig. 3. Structure of near-field resonant coupler (HFSS model)

also allows the radiation from the meander pattern to be reduced. Each element is connected with a co-planar waveguide (CPW) as an I/O interface. In fact, the couplers are built in the PCB to avoid surface discharge [7].

3.2 Design The design parameters of the coupler are shown in Fig. 3. At the first step, we chose a silicon conformal coating ($\varepsilon_r = 2.7$) and set thickness D_1 to 2 mm, which is sufficiently thick compared with a common solder resist, as the cover layer in this research. In addition, thickness D_2 of the core glass epoxy layer ($\varepsilon_r = 4.2$) was temporarily set to 2.4 mm, which is much thicker than the general layer, in order to prevent a partial discharge in the core dielectric [8][9]. Typically, an electric field concentrates at the tip of a sharp-shaped metal. If the electric field intensity exceeds the breakdown strength of an insulator, a partial discharge occurs owing to a local breakdown of the insulator. Therefore, we estimated the maximum electric field intensity in the pattern to determine the line width of the meander pattern M_W. In the ideal case, that of a revolving, projectile-shaped metal tip, the maximum electric field intensity E_{max} at the tip is approximately given by

$$E_{max} = \frac{2V_{ap}}{1.15M_W \log\left(1 + \dfrac{4D_2}{0.5M_W}\right)} \cdots\cdots\cdots\cdots\cdots\cdots (1)$$

where V_{ap} is the applied voltage [10]. We set V_{ap} to 1.65 kV as required for the IGBT operation. We assumed the E_{max} was less than 10 kV/mm which is the actual breakdown voltage of the glass epoxy. We obtained $M_W = 0.12$ mm from the equation since M_W must be minimum for suppressing the parasitic capacitance.

At the second step, to determine the other five parameters, we set target values to have below −20 dB reflection and over

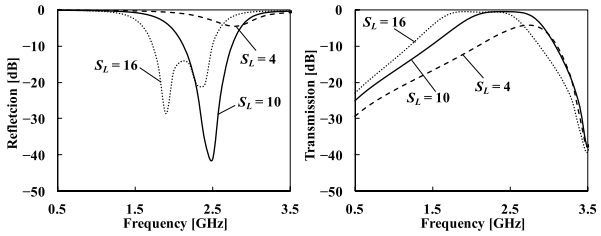

(a) Reflection (b) Transmission

Fig. 4. Simulated characteristics of resonant coupler as function of ground length S_L ($S_W = 14$, $G_W = 1.5$, $M_A = 5.8$, $M_P = 0.4$)

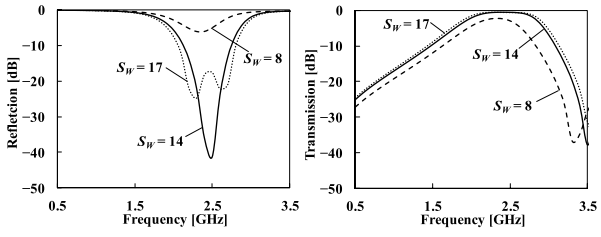

(a) Reflection (b) Transmission

Fig. 5. Simulated characteristics of resonant coupler as function of ground space S_W ($S_L = 10$, $G_W = 1.5$, $M_A = 5.8$, $M_P = 0.4$)

−0.7 dB transmission of the coupler in the 2.4–2.5 GHz frequency range. This transmission target was set so that the whole transmission of the resonant coupler was over −1.0 dB including the −0.3 dB transmission of CPW to microstrip line (MSL) transitions used for matching the interfaces of the couplers and the RF transceivers. To calculate the coupler with the reflection and transmission characteristics, we used HFSS. The reflection was defined as an input reflection at an I/O port of the coupler. This port was connected to a 50-Ω load. The transmission was defined as a power ratio of the output to input. We calculated the sensitivity of five parameters to the reflection and transmission characteristics. These parameters are listed below in Fig. 3:

S_L: Length of ground pattern
S_W: Space between two ground patterns
G_W: Width of ground pattern
M_A: Width of meander pattern
M_P: Pitch of meander pattern

Figure 4 shows the calculated reflection and transmission of the coupler as a function of the ground length S_L. The other four parameters were fixed. As the S_L increases, the coupler resonates at a lower frequency, because a self-inductance L_r of the meander pattern increases with the feeding line for the meander pattern as it gets longer. In addition, the fact that there are two valleys in the reflection characteristic at S_L = 16 mm denotes that the coupler structure has two resonant frequencies. Anti-phase current flows in each element at the lower resonant frequency. On the other hand, the in-phase current flows at the higher one. Moreover, a larger S_L allows the coupler to become more efficient and wider in bandwidth because a capacitance C_g between the two ground patterns increases. Figure 5 shows the characteristics as a function of the ground space S_W. As the S_W decreases, the resonant frequency decreases depending on a capacitance C_s between the

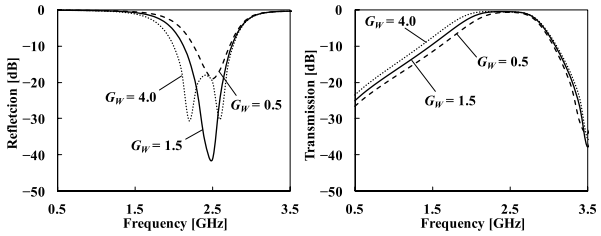

(a) Reflection (b) Transmission

Fig. 6. Simulated characteristics of resonant coupler as function of ground width G_W (S_L = 10, S_W = 14, M_A = 5.8, M_P = 0.4)

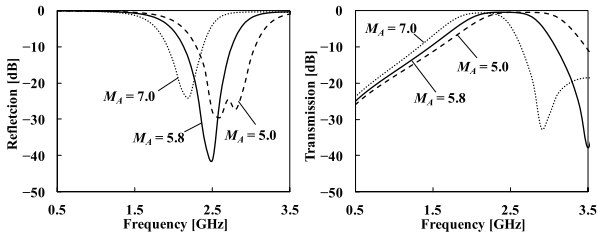

(a) Reflection (b) Transmission

Fig. 7. Simulated characteristics of resonant coupler as function of meander width M_A (S_L = 10, S_W = 14, G_W = 1.5, M_P = 0.4)

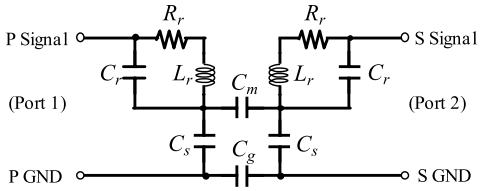

Fig. 8. Equivalent circuit of resonant coupler

meander and ground patterns slightly increasing. Although the distance between the meander and the ground pattern on both sides is shorter when the S_W decreases, the distance between the meander and ground patterns of the CPW is constant. Therefore, there are few changes in the C_s. The figure shows that the level of reflection varies by changing the S_W and has a minimum point. This parameter mainly functions as a component for impedance matching, and the coupler for the S_W = 14 mm has the lowest reflection at 2.4 GHz. Figure 6 shows the influence of the ground width G_W on the characteristics of the coupler. The influence of the G_W has a similar tendency to that of the S_W. A larger G_W enables for the coupler to be even more efficient and a wider bandwidth because the C_g increases. This parameter also contributes to the impedance matching. The influence of the meander width M_A is shown in Fig. 7. As the M_A decreases, the L_r, C_g, and C_s equivalently decreases. All of these behaviors allow the coupler to resonate at a higher frequency. The figure shows two valleys in the reflection characteristic at M_A = 5.0 mm. Although a capacitance C_m between the two meander patterns is small, the coupler could have two resonant frequencies depending on the phase relation between two elements. As for the meander pitch M_P, incidentally, the characteristics are that the resonant frequency becomes monotonically lower with a decreasing M_P due to the small capacitance C_r of the meander pattern. The design results of the characteristics are to be mentioned later.

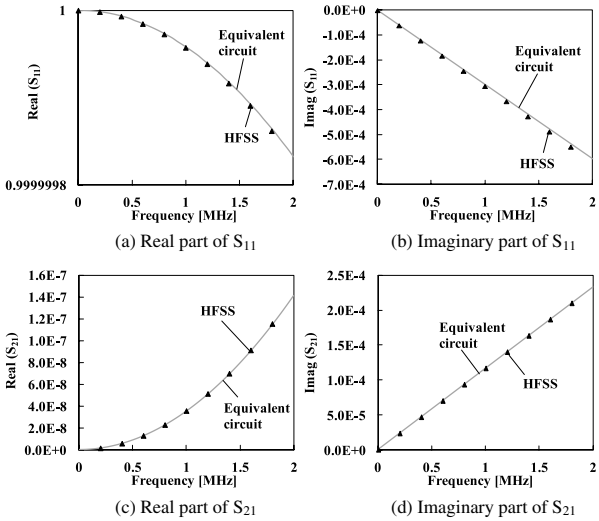

(a) Real part of S_{11} (b) Imaginary part of S_{11}

(c) Real part of S_{21} (d) Imaginary part of S_{21}

Fig. 9. Comparison of S-parameter results using the equivalent circuit and HFSS models

At the third step, we calculated the parasitic capacitance using an equivalent circuit model of the resonant coupler in a low frequency range (≦ 2 MHz), which is important for analyzing the parasitic capacitance. We set a target value to have the parasitic capacitance of less than 1 pF, which is sufficiently small compared with that of a general transformer used for supplying power to the IGBT gate driver. Figure 8 shows the equivalent circuit model we assumed. The meander pattern was modeled as a parallel circuit configured with a self-inductance L_r, a capacitance C_r, and a resistance R_r. In addition, there was a capacitance C_s between the meander and ground patterns. These components allow the element to resonate at a certain frequency. The correspondence of the resonance frequencies of the two elements allows for the resonant coupling through a capacitance C_m between the two meander patterns. A capacitance C_g between the two ground patterns also contributes to the coupling. Increasing capacitances C_m and C_g would improve the coupling efficiency, but could also possibly cause an increase in the noise currents through a parallel circuit configured with C_m and C_g, namely, the parasitic capacitance C_p owing to the IGBT switching. Furthermore, the coupling structure is immune from radiated IGBT disturbances since the elements function as a bandpass filter. In this equivalent circuit, a mutual inductance between two meander patterns need not be considered because the coupling of this structure is determined by the capacitances C_m and C_g. Figure 9 compares S-parameters of the resonant coupler calculated by our equivalent circuit and HFSS models. In our model, we set C_m = 0.32 pF, C_g = 0.44 pF, L_r = 16.63 nH, R_r = 0.11 Ω, C_r = 0.98 pF, and C_s = 0.30 pF. We confirm effectiveness of our model because each S-parameter of our model is in good agreement with one of HFSS model.

At the final step, we made a final decision on the thickness D_2 of the core glass epoxy layer. The thickness D_2 should be chosen in consideration of trade-off between the transmission in the second step and the parasitic capacitance in the third one, as shown in Fig. 10. The trade-off curve obtained by our design method is important to optimize the design of the resonant coupler. In this paper, we chose D_2 = 2.4 mm from the range of D_2 which satisfied the target conditions. At

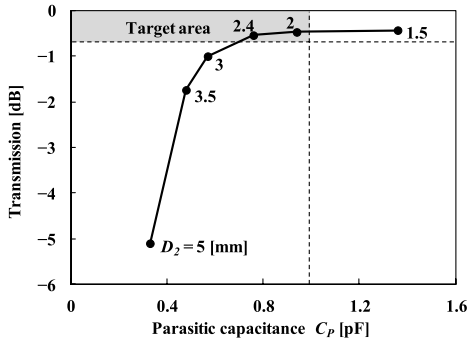

Fig. 10. Relationship between transmission and parasitic capacitance of resonant coupler

Table 2. Parameters of resonant coupler

Parameter	Symbol	Value
Design frequency	f	2.45 GHz
Permittivity of cover dielectric	ε_{r1}	2.7
Permittivity of core dielectric	ε_{r2}	4.2
Thickness of cover dielectric	D_1	2.0 mm
Thickness of core dielectric	D_2	2.4 mm
Line width of meander pattern	M_W	0.12 mm
Length of ground pattern	S_L	10.0 mm
Space between two ground patterns	S_W	14.0 mm
Width of ground pattern	G_W	1.5 mm
Width of meander pattern	M_A	5.8 mm
Pitch of meander pattern	M_P	0.4 mm

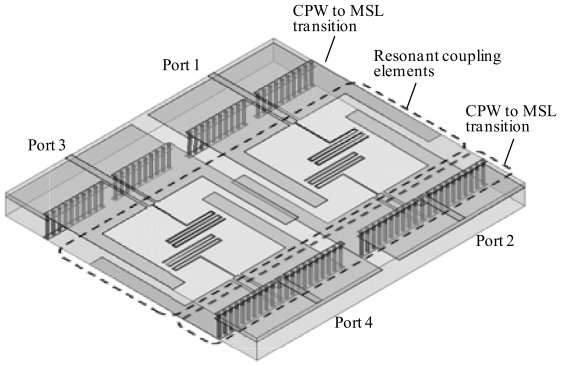

Fig. 11. HFSS model of resonant couplers with I/O adapters

this value, the transmission and the parasitic capacitance C_p were −0.5 dB and 0.76 pF, respectively. Table 2 outlines the design parameters of the coupler.

Figure 11 is the simulation model of the two pairs of couplers as designed above. They are arranged so that they are adjacent to each other. The CPW to MSL transitions are connected to the edges of the resonant coupling elements as I/O adapters. We calculated the reflection, transmission, isolation, and radiation of the couplers as a function of the frequency. The reflection is defined as the input reflection at Port 1, whose characteristic is equal to that of the other ports. All the ports are connected to a 50-Ω load. The transmission is defined as the one from Port 1 to Port 2. The isolation is defined as the ratio of the transmission to the leakage from Port 4 to Port 2. These simulated characteristics are plotted with the measured values in the next section. We observed that the couplers have a band-pass filter characteristic whose

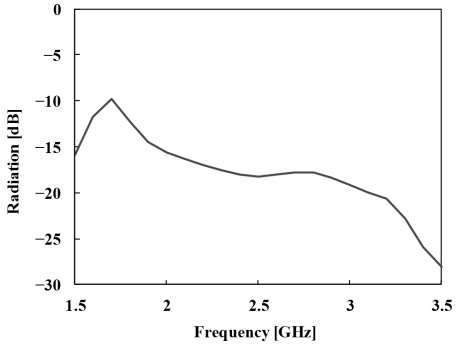

Fig. 12. Simulated radiation characteristic of resonant couplers with I/O adapters

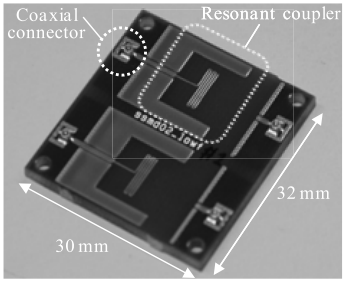

Fig. 13. Photograph of developed resonant couplers with I/O adapters

center frequency is 2.45 GHz. In the 2.4–2.5 GHz frequency range, we obtained a reflection of < −22.6 dB and a transmission of > −0.9 dB, which respectively met the target values. As for the isolation characteristic, we obtained a high isolation of > 38.5 dB in the same frequency band. This value is sufficiently small compared with the target value of > 20 dB in order to avoid any interference between the driving and feedback signals. Figure 12 shows the calculated radiation of the couplers as a function of the frequency. The radiation is defined as the total power radiated from one coupler. We obtained a radiation of under −18.0 dB in the same frequency band. We were able to confirm that the radiation is larger at discontinuous points, such as in the CPW to MSL transitions and the CPW to meander pattern transitions, by monitoring the distribution of the electromagnetic field intensity in the model.

3.3 Experimental Results Figure 13 shows a photograph of the developed resonant couplers, which are 32 mm × 30 mm in area after removing the 2.0-mm-thick silicon conformal coating. The two pairs of couplers are arranged on the first and fourth of the four conductor layers in the PCB. Coaxial connectors are mounted on the PCB to connect the RF transceivers.

Figure 14 plots the measured reflection and transmission characteristics in comparison with the calculated values. We measured the S-parameters after the couplers were connected to the vector network analyzer using coaxial cables. In the 2.4–2.5 GHz frequency range, we obtained a reflection of < −26.4 dB which satisfied the target value. In the same range, however, the transmission was above −1.14 dB, which didn't meet the target value. We would speculate that an actual loss tangent of the glass epoxy was higher than the value of 0.019 we assumed. The slight difference in frequency

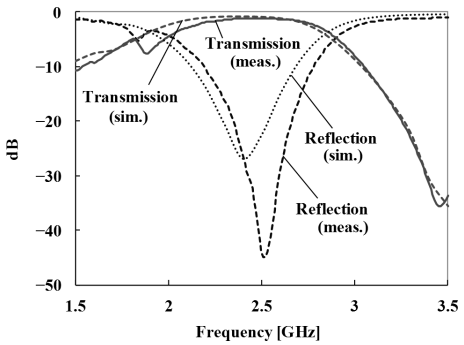

Fig. 14. Measured reflection and transmission characteristics of resonant couplers

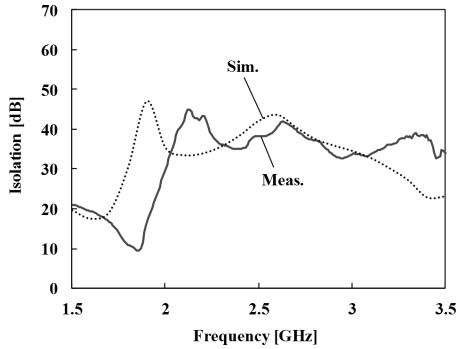

Fig. 15. Measured isolation characteristic of resonant couplers

between the measured and calculated values was caused by the difference in relative permittivity of the coating. Figure 15 plots the measured isolation characteristics with the calculated values. The ports are defined in Fig. 10. The isolation in the operation frequency range of 2.4–2.5 GHz was over 35 dB. The obtained values also satisfied the over 20 dB requirement for the Rx circuit to distinguish the signals from interference. The gap between the measured and calculated values was caused by a large simulation error at the frequency away from the center frequency in addition to the difference in relative permittivity of the coating mention above.

We measured the S-parameters of the resonant coupler to convert them into the parasitic capacitance C_p, after connecting one port to the vector network analyzer and short-circuiting the other three ports. Thus, the resonant couplers were regarded as a series circuit configured with $2R_r$ and C_p located between the measurement port and the ground. Therefore, we could measure C_p from the reactance component of the S-parameter. We adjusted the measured values to compensate for the electrical length of the co-planar waveguide and the coaxial connector. We obtained the parasitic capacitance of 0.80 pF which was close to the value of 0.76 pF calculated by our equivalent circuit model. We were also able to verify the validity of our model experimentally.

Furthermore, we measured the partial discharge of the couplers with or without the silicon conformal coating. We monitored the electric discharge of the couplers in this measurement by applying an AC voltage to the coaxial connectors shown in Fig. 13. The partial discharge inception voltage (PDIV) in this paper is defined as the applied voltage when the electric discharge reached 100 pC. The PDIV for

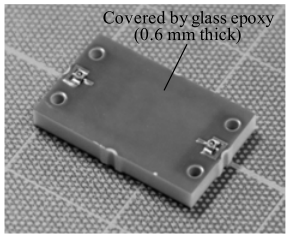

Fig. 16. Photograph of resonant coupler covered by grass epoxy

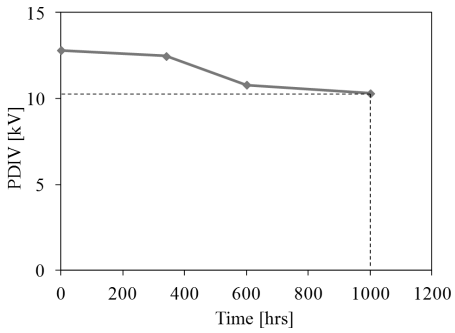

Fig. 17. Measured discharge characteristic of resonant coupler as function of aging time

Table 3. Parameters of resonant coupler

Item	This work	Drive-by- MW [5]	Digital isolator [11]	Optocoupler [12]
Insulation voltage [kV]	10.3	2.5	5.0	5.0
Parasitic capacitance [pF]	0.8	0.42	2.2	0.5
Propagation delay [ns]	38.0	unknown	13.0	150.0

the couplers without the coating was less than 5 kV while no discharge occurred at less than 12 kV for those with coating. This clearly demonstrates that the coating helps to avoid any electric discharge along the dielectric surface. We performed an accelerated aging test to ensure the insulation reliability of the couplers. The couplers were exposed to a temperature-humidity- bias test at 85°C and 85% rel. A DC bias voltage of 3.3 kV was simultaneously applied between the connectors on the primary and secondary sides. Figure 16 shows a photograph of the coupler as the test sample. The 0.6-mm-thick cover layer is made of the same glass epoxy as the core layer. Figure 17 plots the PDIV characteristic of the test sample as a function of the accelerating time. The PDIV, which was 12.8 kV before the test, gradually decreased as the accelerating time elapsed. At 1000 hours, however, we confirmed the PDIV was 10.3 kV, which was sufficiently higher compared to the target value of 3.3 kV, and demonstrated excellent coupler reliability.

Table 3 compares the performance obtained in this work with other technologies. Our insulated communication module has the insulation voltage of 10.3 V, which is the highest. This is presumably because the core and the cover dielectric effectively prevent the partial and the surface discharge. As for the parasitic capacitance and the propagation delay, our module has intermediate values of the Digital isolator and the Optocoupler. In order to further reduce the parasitic capacitance of our module, it is effective to reduce the size of the coupler and add a Tx amplifier to compensate for the

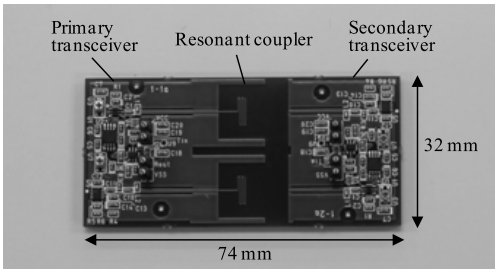

Fig. 18. Photograph of insulated communication module

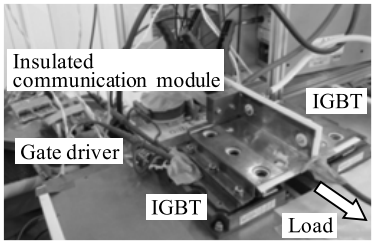

Fig. 19. Experimental setup of IGBT operated by insulated communication module

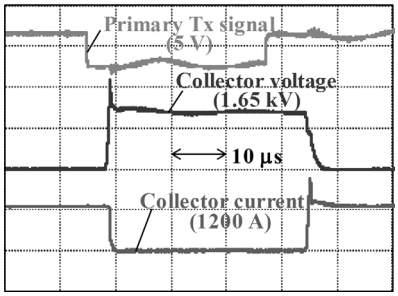

Fig. 20. Measured IGBT switching waveforms

deteriorated transmission loss. As for the propagation delay, it is possible to reduce the delay by adopting high-speed circuit components though it is a trade-off with cost.

4. Measurement of Insulated Communication Module

Figure 18 shows a photograph of the insulated communication module we developed. The primary and secondary transceivers in the module configured with the couplers occupy a 32 mm × 74 mm area on the PCB which, like the couplers shown in Fig. 13, has four conductor layers. We confirmed that this module had a propagation delay of 38.0 ns from the input of the primary transceiver to the output of the secondary one.

We performed an IGBT switching operation experiment by using the insulated communication module shown in Fig. 19. The 3.3 kV–1200 A IGBTs were connected to the gate driver and the insulated communication module. A large-sized coil and capacitor were used to provide a load equivalent to that of a motor. The measured waveforms obtained in the operation (Fig. 20) confirmed that our developed module functions correctly, and thus, demonstrated that it is possible to transmit driving signals via insulated communication without disturbances between the high power switching IGBTs and RF transceivers. We confirmed that the observed delay of several microseconds mostly occurred in the gate driver. In our future work we plan to use our technology to supply power to the IGBT gate driver and integrate the power supply with the signal transmission [13][14].

5. Conclusion

We developed an insulated signal transmission system using a near-field resonant couplers for providing driving signal transmission to control power switching devices such as IGBTs. In this paper, we focused a parasitic capacitance of the resonant coupler because the capacitance needs to be reduced for suppression of the noise current caused by IGBTs. We introduced an equivalent circuit model of the resonant coupler to simulate the capacitance, and showed a validity of our model by confirming agreement between the calculated value of 0.76 pF and the measured value of 0.80 pF. An insulated communication module that consists of the resonant couplers, the primary and secondary transceivers on the PCB was fabricated. The module demonstrated the switching operation of 3.3 kV–1200 A IGBTs without disturbances between the high power switching IGBTs and the RF transceivers.

Acknowledgment

The authors are indebted to Mr. J. Kusukawa and Dr. J. Sakano of Hitachi, Ltd., for assisting them with the IGBT operation and the partial discharge experiments and for the many helpful discussions we had with them.

References

(1) M. Hornkamp, S. Pawel, and O. Garcia: “Latest Generation IGBT Gate Drivers”, Power Systems Design Europe Magazine, pp.21–23 (2009)
(2) J. Thalheim and O. Garcia: “Highly Flexible and Low-Cost Gate Driver Cores for Voltage Classes of up to 3300 V”, Bodo’s Power Systems Magazine, pp.26–27 (2009)
(3) S. Brehaut, F. Costa, J. Casarin, and B. Chauchat: “Gate driving of a 3.3 kV IGBT chopper by an 8 bits encoded wireless transmission”, Proc. PCIM Europe, S3b-2 (2007)
(4) C. Batard, G. Andrieux, N. Ginot, and M.A. Mannah: “Wireless Transmission of IGBT Driver Control”, APEC 2009. Twenty-Fourth Annual IEEE, pp.1257–1262 (2009)
(5) S. Nagai, Y. Kawai, O. Tabata, H. Fujiwara, N. Otsuka, D. Ueda, N. Negoro, and M. Ishida: “A Compact Drive-by-Microwave Gate Driver with Coupler Integrated in a Package”, APEC 2014, pp.1461–1464 (2014)
(6) H. Shinoda and T. Terada: “Insulated Signal Transmission System using Planar Resonant Coupling Technology for High Voltage IGBT Gate Driver”, ECCE 2014, pp.265–270 (2014)
(7) C. Heitz, M. Piemontesi, and G. Salge: “Surface Discharge along Solid Dielectrics in Atmospheric Air”, Electrical Insulation, Conference Record of the 2000 IEEE International Symp., pp.341–344 (2000)
(8) S. Pawel and J. Thalheim: “1700 V Fully Coreless Gate Driver with Rugged Signal Interface and Switching-Independent Power Supply”, ISPSD 2008. 20th International Symp, pp.319–322 (2008)
(9) S. Pawel and J. Thalheim: “1700 V Planar Transformers for High Power Gate Drives”, Proc. PCIM Europe, pp.753–758 (2009)
(10) J.H. Mason: “The Deterioration and Breakdown of Dielectrics Resulting from Internal Discharges”, Proc. IEE Part I General Vol.98, pp.44–59 (1951)
(11) ADuM220N Data Sheet Rev. A, http://www.analog.com
(12) ACNW3430 Data Sheet, http://www.avagotech.com
(13) S. Timothe, R. Nicolas, C.J. Christophe, and A.J. Daniel: “Design and Characterization of a Signal Insulation Coreless Transformer Integrated in a CMOS Gate Driver Chip”, ISPSD 2011. 23th International Symp, pp.360–363 (2011)
(14) R. Wu, J.K.O. Sin, and S.Y. Hui: “A Novel Silicon-Embedded Coreless Transformer for Isolated DC-DC Converter Application”, ISPSD 2011. 23th International Symp, pp.352–355 (2011)

Hiroshi Shinoda (Non-member) received his B.E. in Physical Electronics from the Tokyo Institute of Technology, Tokyo, Japan in 1998. The same year, he joined the Central Research Laboratory, Hitachi Ltd., Tokyo, Japan. From 1998–2009, he was engaged in the research and development of millimeter-wave antennas and Direction of Arrival (DOA) estimation techniques for automotive radars. Since 2010, he has been engaged in the research on wireless power transmission and wireless communication systems.

Takahide Terada (Non-member) received his B.S., M.S., and Ph.D. degrees in electrical engineering from Keio University, Yokohama, Japan, in 2003, 2005, and 2015. In 2005, he joined the Central Research Laboratory, Hitachi Ltd., Tokyo, Japan, where he has been engaged in the research and development of low-power CMOS RF circuits for ultra-wideband impulse radio. He has also been engaged in research on high-speed and high-accuracy CMOS mixed-signal circuits for HDD read channel and MCU. From 2010 to 2014, he was engaged in the research on wireless power transmission and data communication systems for industrial equipment and vehicles. His current research interests include mixed-signal circuits and systems for medical equipment. Dr. Terada was a recipient of the 2014 APEC (Applied Power Electronics Conference and Exposition) Outstanding Presentation Award.